The supplement of Laminar gas inlet – Part 2: Wind tunnel chemical transmission measurement and modelling

Da Yang[1,2,3,*], Emmanuel Assaf[4], Roy Mauldin[4], Suresh Dhaniyala[3] , and Rainer Volkamer[1,2,4,*]

[1]Department of Chemistry, University of Colorado Boulder, Boulder, CO
[2]Cooperative Institute for Research in Environmental Sciences (CIRES), University of Colorado Boulder, Boulder, CO
[3]Mechanical and Aeronautical Engineering, Clarkson University, Potsdam, NY
[4]Dept of Atmospheric and Oceanic Sciences, University of Colorado Boulder, Boulder, CO

*Correspondence to: Da Yang (da.yang@colorado.edu); Rainer Volkamer (rainer.volkamer@colorado.edu)

During the four-day measurement period, the specific humidity in the air changed over time. As shown in Figure S1a, the specific humidity (q) has a large variation at different measurement periods. H_2SO_4 $NCPS$ measurement results were obtained by calculating the differences between raw data in signal mode and background mode. The repeated measurement results are shown in Figure S1b. We calculate standard uncertainty to describe our error and propagate our uncertainty for H_2SO_4 $NCPS$. The H_2SO_4 $NCPS$ of these repeated measurements has significant variation, with a ~40% difference, at different measurement periods (Fig. S1b left y-axis). By Normalizing the H_2SO_4 $NCPS$ using the factor of specific humidity (f_q), the difference among three repeated measurements is largely reduced to a ~15% difference (Fig. S1b right y-axis).

The sample flow features in the effective illuminated area are correlated with freestream flow velocity and size of restrictor. As shown in Figure S2a, the inlet reduces the freestream velocity to a much lower level inside the inner shroud, and a direct correlation can be seen between the freestream flow velocity (U_∞) and the sample flow velocity at the effective light area (U_{light}). Meanwhile at the same area, the radius of the sample flow shows the opposite correlation with the freestream velocity. In addition, the smaller size of restrictor results in a lower sample flow velocity (U_{light}) and a larger sample flow radius at the effective light area. A further investigation of the sample flow radius at the effective light area, as shown in Figure S2b , reveals a direct correlation between the radius of sample flow and the ratio of flow velocity at the sampling tube entrance ($U_{entrance}$) over the light area (U_{light}). Reducing the velocity ratio, $U_{entrance}/U_{light}$, can enlarge the radius of sample flow passing through the effective light area and result in generating more OH radical source.

When the sample flow is entering the sampling tube, the flow velocity slows further and results in an increase of turbulent intensity. Using our previous CFD simulation results (Yang et al., 2024), as shown in Figure S3, all simulation cases from both restrictors (12.5mm & 17mm) show that the enhancement of sample flow turbulent intensity directly inside the sampling tube, i.e., the ratio of the turbulent intensity inside the sampling tube entrance ($TI_{15}°$) to the incoming flow turbulent intensity (T_A),

decreases as the ratio between flow velocity at sampling tube entrance and the incoming flow velocity ($U_{entrance}/U_A$) increases.

Since the sample flow in the aircraft inlet section is mainly impacted by the upstream flow conditions, the gas sampling efficiency of the aircraft inlet from both altitudes and both species can be approximately merged into one trend by using the flow rate divided by the laminar diffusivity as a new variable (Fig. S4).

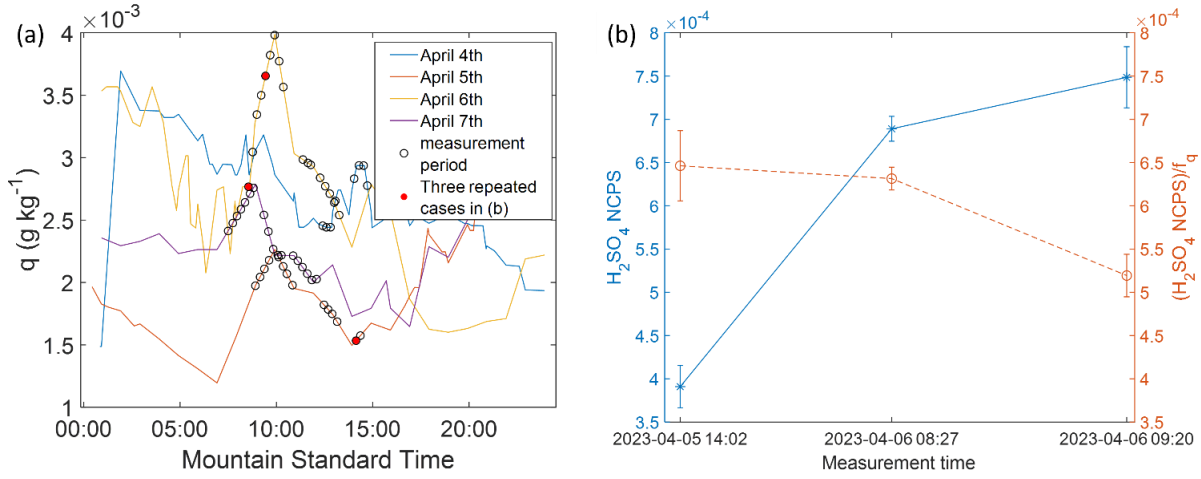

Figure S1. (a) The results of specific humidity (q) at different periods. The circles mark the average time of each period. The red circles mark the three repeated measurement periods in (b). (b) The results of H_2SO_4 *NCPS* compared to the H_2SO_4 *NCPS* results normalized by the factor of specific humidity (f_q). Three different measurement periods in (b) are operated at 30 $m\ s^{-1}$ freestream velocity with 12.5mm restrictor, 4 SLPM sampling flow rate and type 1 transmission line. The error bar is data uncertainty which follows section 2.4.

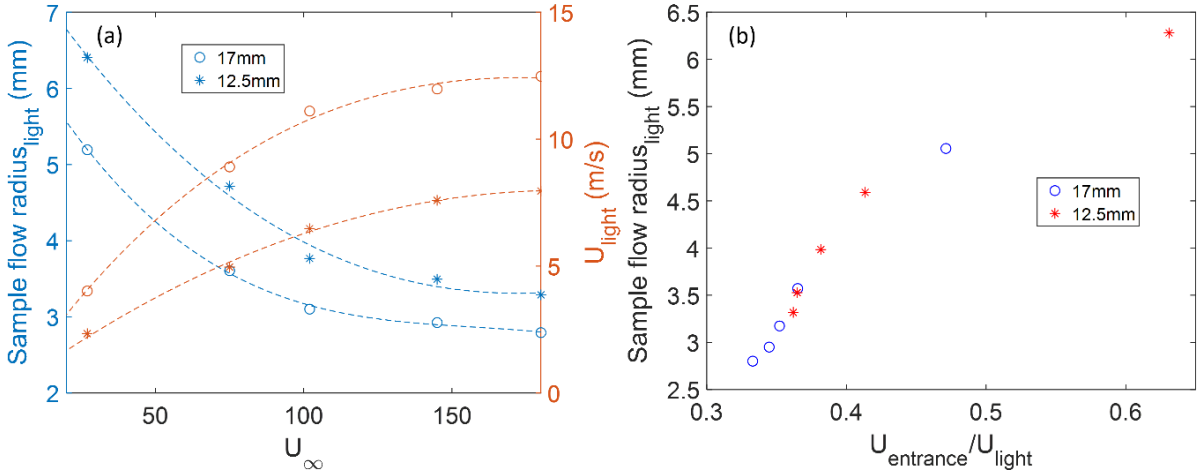

Figure S2. The simulation results of sampling flow features at effective illumination area under same sampling flow velocity 2.4 $m\ s^{-1}$. (a) The correlation between freestream velocity U_∞ and flow features at effective light area. The left y axis shows the average

radius of sample flow passing the light area; the right y axis shows the average sample flow velocity U_{light} in the same area. (b) The relationship between the sample flow radius at effective illuminated area and the entrance velocity ratio, i.e., the flow velocity at the entrance of sampling tube $U_{entrance}$ divided by the flow velocity at the light area U_{light}.

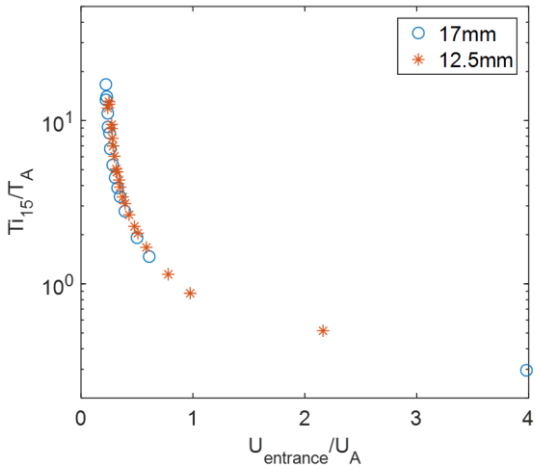

Figure S3. Correlation between the turbulent intensity enhancement directly inside the sampling tube entrance and flow velocity ratio among all inlet simulation cases from previous study. The turbulent intensity enhancement is calculated using the turbulent intensity inside the sampling tube entrance T_{15° divide the incoming flow turbulent intensity T_A. The flow ratio is calculated using the flow velocity at the entrance of the sampling tube $U_{entrance}$ divided by the incoming flow velocity U_A. All subscripts described the reference locations in previous paper (Yang et al., 2024).

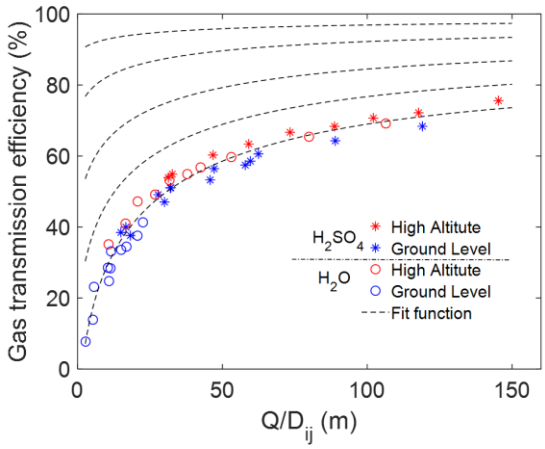

Figure S4. The unified correlation of gas sampling efficiency for both water vapor and gas-phase H_2SO_4 in the aircraft inlet section. The x axis has the volume flow rate in ($m^3\ s^{-1}$). divided by laminar diffusivity ($m^2\ s^{-1}$). The star marker presents gas-phase H_2SO_4 , the circle marker presents water vapor. The blue presents the ground level condition (970 mbar ambient pressure), the red presents the high-altitude condition (150 mbar ambient pressure). The dashed line is the fit function with different selections of mass accommodation coefficients (α_i).